APPLIED COMPUTATIONAL ELECTROMAGNETICS SOCIETY JOURNAL

April 2018
Vol. 33 No. 4
ISSN 1054-4887

The ACES Journal is abstracted in INSPEC, in Engineering Index, DTIC, Science Citation Index Expanded, the Research Alert, and to Current Contents/Engineering, Computing & Technology.

The illustrations on the front cover have been obtained from the research groups at the Department of Electrical Engineering, The University of Mississippi.

EMERITUS ASSOCIATE EDITORS-IN-CHIEF

EMERITUS EDITORIAL ASSISTANTS

APRIL 2018 REVIEWERS: REGULAR PAPERS

Mohammad Alibakhshikenari
Stamatios Amanatiadis
Zsolt Badics
Subbarao Bandaru
Cemile Bardak
Thomas Bauernfeind
Marek Bleszynski
Bair Budaev
Mohammed Hadi
Zhixiang Huang
Irum Jafri
Mario Jakas
Ulrich Jakobus
Ming Jin
Angelo Liseno
Biswajeet Mukherjee
Sovanlal Mukherjee
Imaculate Rosaline
Esther S.
Christoph Statz
Candace Suriano
Aathmanesan T.
Yuvaraja T.
Qi Wu
Zubiao Xiong
Rengan Xu
Ravindra Yadav
Ferdows Zarrabi

APRIL 2018 REVIEWERS: EXPRESS PAPERS

Robert Burkholder
Fangyuan Chen

THE APPLIED COMPUTATIONAL ELECTROMAGNETICS SOCIETY JOURNAL

Vol. 33 No. 4 April 2018

TABLE OF CONTENTS – REGULAR PAPERS

Temperature Rise and SAR Distribution at Wide Range of Frequencies in a Human Head due to an Antenna Radiation
Fatih Kaburcuk and Atef Z. Elsherbeni 367

Modulation of the Antenna-Head Interaction inside a Closed Environment Using MOM-GEC Method
Hafawa Messaoudi and Taoufik Aguili 373

Design and Measurements of Rectangular Dielectric Resonator Antenna Linear Arrays
Feras Z. Abushakra, Asem S. Al-Zoubi, and Derar F. Hawatmeh 380

Design, Fabrication, and Measurements of Extended L-Shaped Multiband Antenna for Wireless Applications
Ashfaq Ahmad, Farzana Arshad, Syeda I. Naqvi, Yasar Amin, and Hannu Tenhunen 388

A Novel Dielectric Loaded Vivaldi Antenna with Improved Radiation Characteristics for UWB Application
Hua Zhu, Xiuping Li, Li Yao, and Jun Xiao 394

A New Compact Planar Antenna for Switching between UWB, Narrow Band and UWB with Tunable-notch Behaviors for UWB and WLAN Applications
Mansour NejatiJahromi, Mahdi NagshvarianJahromi, and MuhibUr Rahman 400

High-Resolution Ultra-Wideband Material Penetrating Radar (UWB-MPR) using Modified Configuration of Receiver Antennas
Mohammad Ojaroudi and Hashem Jahed 407

Dual Layer Convoluted Frequency Selective Surface Design in the 2.4 GHz and 5.8 GHz ISM Bands
Bora Döken and Mesut Kartal 413

Near to Far-Field Plane-Polar Transformation from Probe Positioning Error Affected Data
Francesco D'Agostino, Flaminio Ferrara, Claudio Gennarelli, Rocco Guerriero, and Massimo Migliozzi 419

High-order Staggered Finite Difference Time Domain Method for Dispersive Debye Medium
Ammar Guellab and Wu Qun 430

Effective CFS-PML Formulations Based on 2-D TE phi BOR-FDTD for the Drude Model
Jianxiong Li and Wei Jiao 438

Complex-Envelope ADE-LOD-FDTD for Band Gap Analysis of Plasma Photonic Crystals
Tu-Lu Liang, Wei Shao, and Sheng-Bing Shi 443

FPGA Based Fast Bartlett DoA Estimator for ULA Antenna Using Parallel Computing
Fahri M. Unlersen, Ercan Yaldiz, and Sehabeddin T. Imeci 450

TABLE OF CONTENTS – EXPRESS PAPERS

Experimental Characterization of an All-Dielectric Metasurface with Optical Activity Properties
Ali Yahyaoui and Hatem Rmili 460

A Direct Solver Based on Rank-Structured Matrix for Large Arrays in Method of Moment
Weikang Yu, Hu Yang, Shengguo Li, and Yanlin Xu 464

Experimental Characterization of an All-Dielectric Metasurface with Optical Activity Properties

Ali Yahyaoui [1,2] and Hatem Rmili [1]

[1] King Abdulaziz University
Electrical and Computer Engineering Department, P.O. Box 80204, Jeddah 21589, Saudi Arabia
hmrmili@kau.edu.sa

[2] University of Jeddah
Electrical and Computer Engineering Department, PO. Box 80327, Jeddah 21589, Saudi Arabia

Abstract ─ A new microwave all-dielectric metasurface based on elliptic dielectric resonators (EDRs) with optical activity properties was fabricated and characterized experimentally. The 5.12 mm-thick metasurface is composed of two layers of connected elliptic dielectric resonators (Rogers RO3210) with elliptic slots and was excited with two orthogonal polarizations of the incident electric field. The optical activity was studied through two constitutive parameters representing the rotation angle θ and polarization state (η) of incident and transmitted electric fields through the metasurface. It is found that the proposed design may rotate the incident linearly polarized electric fields over many frequency bands with different transmissions levels. The obtained performances may offer to the device the possibility to be used as microwave polarization rotator.

Index Terms ─ Dielectric metasurface, optical activity, polarization state.

I. INTRODUCTION

Metamaterials [1,2] and metasurfaces [3] have emerged as potential devices for the control of transmission of electromagnetic waves in terms of amplitude, phase and polarization.

In particular, all-dielectric metasurfaces have attracted much attention due mainly to their low losses at high frequencies such as the visible and near-infrared spectral bands [3]. In addition, their high overall efficiency and various functionalities have permitted their use to develop innovative devices for different microwave, THz and optical applications [3]. The operating principle of all-dielectric metasurfaces consists on the use of dielectric resonators to excite both electric and magnetic resonant modes; and usually we use spheres, cubes, cylindrical/elliptical disks and rods with high dielectric constant to reduce the metasurface size.

On the other hand, chiral metasurfaces are emerging as new devices with original electromagnetics properties such as optical activity [4], and circular dichroism [5], which are significantly higher than higher natural chiral materials. The optical activity which describes the rotation angle between the polarization planes of the transmitted and incident waves, was widely obtained with conventional metallic metasurfaces, but rarely with all-dielectric ones.

For this reason, we have studied experimentally in this letter, the optical activity of an all-dielectric metasurface based on elliptic dielectric resonators operating at microwave frequencies. Recently, we have proved that these resonators are good candidates for the design of Quarter-Wave Plate (QWP) and Half-Wave Plate (HWP) all-dielectric metasurfaces [6-8], and in this letter, we propose their use to obtain all-dielectric metasurfaces with optical activity behavior in the frequency band 10-20 GHz.

II. METASURFACE DESIGN AND ANALYSIS

A. Simulation model

We have designed a 5.12 mm-thick all-dielectric metasurface (Fig. 1) by using two superposed arrays of dielectric resonators made of Rogers RO3210 of permittivity $\varepsilon_r = 10.2$, and loss tangent $\tan\delta = 0.0027$. Each array of thickness 2.56 mm is composed of connected elliptic resonators of minor radius a, major radius b and ellipticity τ=b/a, with elliptic slots of minor radius a_s, major radius b_s and ellipticity $\tau_s = b_s / a_s$. We have rotated the resonators composing the upper and lower arrays are around their z-axis with angles ϕ= -25° and - ϕ = 25°, respectively as shown in Fig. 1, and connected them along x-direction with thin strips of length $L_c = (L_x/2)$-b and width W_c = 1.25 mm.

Each unit cell (Fig. 1) of size $L_x \times L_y$ (L_x = 3 mm,

Submitted On: January 22, 2018
Accepted On: March 7, 2018

L_y = 2 mm) contains two superposed dielectric resonators of same size but with different orientations (-ϕ and + ϕ for the upper and lower resonators, respectively).

The fabricated all-dielectric metasurface of dimensions 74.5 × 74.5 mm^2 is composed of 5 × 5-unit cells made of Rogers RO3210 as shown in Fig. 2. The total height of 5.12 mm corresponds to two layers of resonators of thickness 2.56 mm.

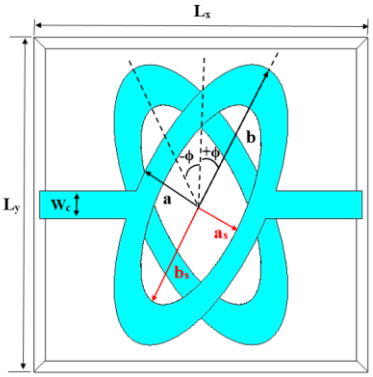

Fig. 1. CST-model for the unit cell.

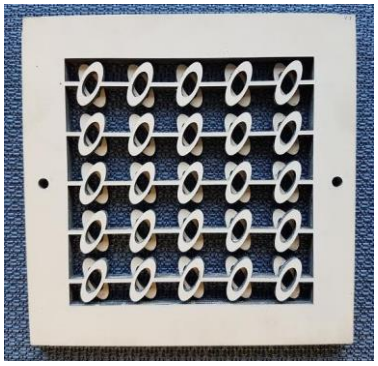

Fig. 2. Photo of the realized metasurface.

B. Metasurface analysis

The optical activity can be analyzed with two constitutive parameters; the azimuth rotation angle θ, and the polarization state η [9]:

$$\theta = [\arg(T_{++}) - \arg(T_{--})]/2, \quad (1)$$

$$\eta = \tfrac{1}{2} \arcsin [(|T_{++}|^2 - |T_{--}|^2) / (|T_{++}|^2 + |T_{--}|^2)], \quad (2)$$

where T_{++} and T_{--} are the transmitted coefficients of right-hand circularly polarized (RCP) and left-hand circularly polarized (LCP) waves, respectively.

We can determine the coefficients T_{++} and T_{--} from the linear transmission coefficients T_{xx}, T_{xy}, T_{yx} and T_{yy} by using the following equations [9]:

$$T_{++} = \frac{1}{2}[(T_{xx} + T_{yy}) + i(T_{xy} - T_{yx})], \quad (3)$$

$$T_{--} = \frac{1}{2}[(T_{xx} + T_{yy}) - i(T_{xy} - T_{yx})], \quad (4)$$

where, $T_{xx} = \frac{E_x^t}{E_x^i}$, $T_{xy} = \frac{E_x^t}{E_y^i}$, $T_{yx} = \frac{E_y^t}{E_x^i}$ and $T_{yy} = \frac{E_y^t}{E_y^i}$.

Here, the first subscript represents transmitted polarizations, and the second subscript denotes the incident ones.

C. Design procedure

First, we have numerically studied the structure with the commercial software CST Microwave Studio by exciting it under normal incidence and by taking periodic boundary conditions along x- and y-directions.

Next, we have identified the main design parameters affecting the metasurface performances which are the ellipticities τ and τ_s of the resonator and the slot, respectively, and the orientation ϕ of the resonator. These parameters were optimized to improve the metasurface optical activity described by Eqs. (1) and (2), within the band 10-20 GHz.

Finally, we have optimized parameters τ and ϕ for the metasurface without slot, and the parameter τ_s when we have added the slot. So, the optimized values giving good optical activity in terms of azimuth rotation angle θ, and polarization state η [9] are a=3 mm, b=7 mm, a_s=2 mm, b_s=4 mm giving resonator and slot ellipticities of τ=2.33 and τ_s=2, and rotation angles ϕ = ±25°. Details on the parametric study can be found in [10].

III. RESULTS AND DISCUSSIONS

Fabrication of the final prototype and measurements of the metasurface transmission coefficients (amplitude and phase) were performed at the University of Montreal in Canada (Dr. Christophe Caloz research, Ecole Polytechnique de Montréal) by using the home-made measurement setup [7].

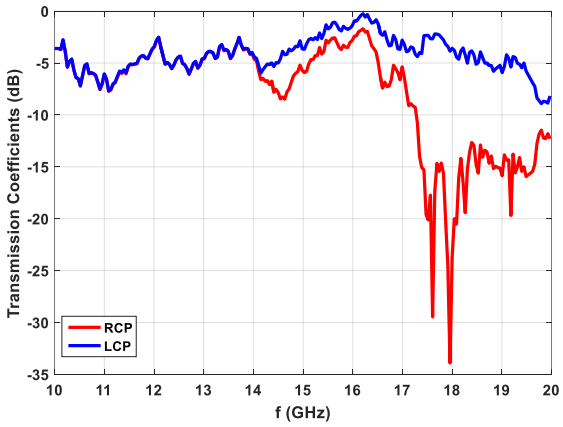

Fig. 3. Variation of the experimental RCP and LCP transmission coefficients over the frequency band 10-20 GHz.

In Fig. 3, we have superposed moduli of both RCP and LCP transmitted coefficients for the realized prototype over the frequency band 10-20 GHz. These moduli were obtained from measured linear transmission

coefficients T_{xx}, T_{xy}, T_{yx} and T_{yy}, where the first and second subscripts denotes transmitted and incident polarizations, respectively.

Analysis of the curves presented in this Fig. 3, shows that RCP and LCP moduli are equal up to 14.1 GHz, whereas for higher frequencies, a visible difference between them is observed, which means that the pure optical activity ($|\eta|\approx 0°$) may appear only for frequencies lower than 14. 1 GHz. However, an optical activity with small ellipticity ($|\eta|<10°$) can be achieved for upper frequencies with a slight tendency to transmit LCP waves more than RCP ones ($\eta<0$).

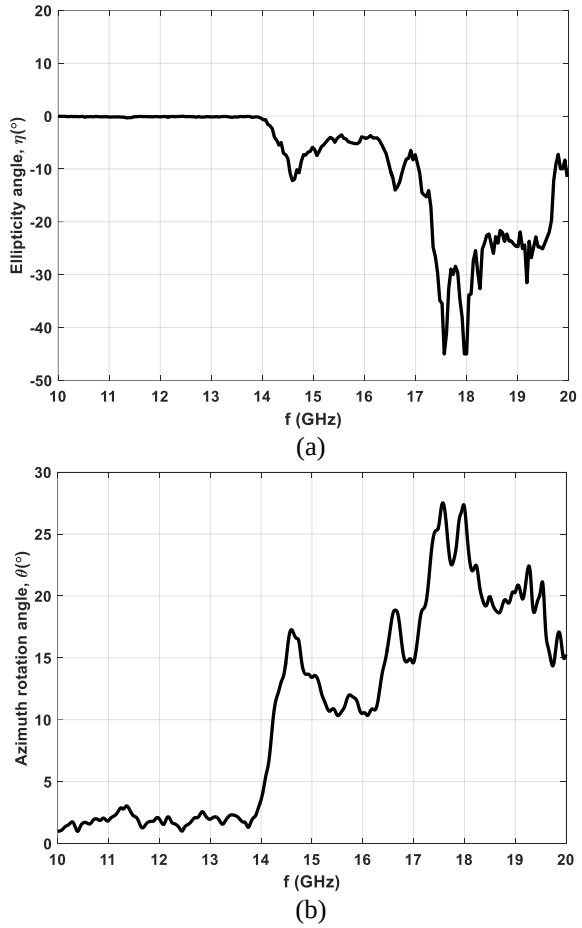

Fig. 4. Variation of the measured parameters over the frequency band 10-20 GHz: (a) polarization state η, and (b) azimuth rotation angle θ.

To better analysis the metasurface optical activity, we have given in Fig. 4 the experimental constitutive parameters (η and θ) evolution with the frequency, and the main related data are resumed in Table 1.

We can notice from Table 1, that a small and wideband (33.3%) pure optical activity can be obtained over the band 10-14 GHz; for example, an optical activity of 8° per wavelength at 10.17 GHz, with transmission level of 77%. However, by considering optical activity with small ellipticity ($|\eta|<10°$), we can achieve higher values such as 66° per wavelength with transmission levels of 42% and 63%, for RCP and LCP waves, respectively at 14.54 GHz within a large frequency range (14.68-16.51 GHz) of fractional bandwidth 2%.Also, we can get higher transmission levels (i.e., 83% and 96%, for RCP and LCP waves, respectively at 16.16 GHz) over less wider frequency band (11.73%) but with lower optical activity (39° per wavelength).

Table 1: Main results deduced from Fig. 3 and Fig. 4, related to the metasurface optical activity

Ellipticity	Range (GHz) Bandwidth (%)	Transmission Level	Optical Activity (Degrees/ Wavelength)
$\|\eta\|\approx 0°$	10-14 (33.33%)	75% @ 10.17 GHz 77% @ 12.1 GHz 77% @ 13.71 GHz	8 @ 10.17 GHz 7 @ 12.1 GHz 6 @ 13.71 GHz
$\|\eta\|<10°$	10-14.54 (37%)	42% for RCP 63% for LCP @ 14.54 GHz	66 @ 14.54 GHz
	14.68-16.51 (11.73%)	83% for RCP 96% for LCP @ 16.16 GHz	39 @ 16.16 GHz
	16.73-17.08 (2%)	51% for RCP 71% for LCP @ 16.77 GHz	56 @ 16.77 GHz
	19.73-19.96 (1.15%)	30% for RCP 41% for LCP @ 19.87 GHz	50 @ 19.87 GHz

IV. CONCLUSION

We have fabricated a multiband all-dielectric metasurface based on EDRs with optical activity performances bands within the range 10-20 GHz. The meta-device can rotate an incident linearly polarized wave with relatively good transmission levels and the transmitted waves lose only slightly their linearity. The optimum cases correspond to the frequency 14.54 GHz, where the metasurface shows the highest optical activity (66° per wavelength) with moderate transmission levels, and the frequency 16.16 GHz where transmission levels are higher but with lower optical activity (56° per wavelength).

The proposed metasurface design may be a good solution for the design of all-dielectric devices such as polarization rotator operating at microwave frequencies.

ACKNOWLEDGMENT

This project was funded by the Deanship of Scientific Research (DSR) at King Abdulaziz University, Jeddah, under Grant No. (RG-2-135-38). The authors, therefore, acknowledge with thanks DSR for technical and financial support.

REFERENCES

[1] F. Karadag, İ. Çomez, F. Dincer, M. Bakır, and M. Karaaslan, "Dynamical chiral metamaterial with giant optical activity and constant chirality over a certain frequency band," *ACES Journal*, vol. 31, no. 8, pp. 919-925, Aug. 2016.

[2] I. Comez, M. Karaaslan, F. Dincer, F. Karadag, and C. Sabah, "Systematic analysis on the optical properties of chiral metamaterial slab for microwave polarization control," *ACES Journal*, vol. 35, no. 5, pp. 478-487, May 2015.

[3] H. T. Chen, A. J Taylor, and N. Yu, "A review of metasurfaces: Physics and applications," *Reports on Progress in Physics*, vol. 79, no. 7, June 2016.

[4] J. Zhou, D. R. Chowdhury, R. Zhao, A. K. Azad, H. Chen, C. M. Soukoulis, A. J. Taylor, and J. F. O'Hara, "Terahertz chiral metamaterials with giant and dynamically tunable optical activity," *Phys. Rev.* B, 86(3), 035448,, 2012.

[5] Y. Cheng, Y. Nie, Lin Wu, and R. Gong, "Giant circular dichroism and negative refractive index of chiral metamaterial based on split-ring-resonators," *Progress in Electromagnetics Research*, vol. 138, pp. 421-432, 2013.

[6] A. Yahyaoui, H. Rmili, K. Achouri, M. Sheikh, A. Dobaie, and T. Aguili, "Transmission control of electromagnetic waves by using quarter-wave plate and half-wave plate all-dielectric metasurfaces based on elliptic dielectric resonators," *International Journal on Antennas and Propagation*, vol. 2017, Article ID 8215291, 8 pages, 2017.

[7] K. Achouri, A. Yahyaoui, S. Gupta, H. Rmili, and C. Caloz, "Dielectric resonator metasurface for dispersion engineering," *IEEE Trans. Antennas. Propag.*, vol. 62, no. 2, pp. 673-680, Feb. 2017.

[8] A. Yahyaoui, H. Rmili, M. Sheikh, A. Dobaie, L. Laadhar, and T. Aguili, "Design of all-dielectric half-wave and quarter-wave plates microwave metasurfaces based on elliptic dielectric resonators," *ACES Journal*, vol. 32, no. 3, pp. 229-236, Mar. 2017.

[9] J. D. Jackson, *Classical Electrodynamics*. 3rd Edition, Wiley, 1999.

[10] A. Yahyaoui and H. Rmili, "Chiral all-dielectric metasurface based on elliptic resonators with circular dichroism behavior," *International Journal on Antennas and Propagation*, vol. 2018, Article ID 6352418, 7 pages, 2018.

Ali Yahyaoui received the master degree in Electrical and Electronics from the University of Tunis El Manar, Faculty of Sciences, in 2012. He is currently working toward the Ph.D. degree in Communication System at the National Engineering School of Tunis (ENIT), University of Tunis El Manar.

His areas of interests are antenna designs, metamaterials and metasurfaces.

Hatem Rmili received the B.S. degree in General Physics from the Science Faculty of Monastir, Tunisia in 1995, and the DEA diploma from the Science Faculty of Tunis, Tunisia, in Quantum Mechanics, in 1999. He received the Ph.D. degree in Physics (Electronics) from both the University of Tunis, Tunisia, and the University of Bordeaux 1, France, in 2004.

From December 2004 to March, 2005, he was a Research Assistant in the PIOM Laboratory at the University of Bordeaux 1. During March 2005 to March 2007, he was a Postdoctoral Fellow at the Rennes Institute of Electronics and Telecommunications, France. From March to September 2007, he was a Postdoctoral Fellow at the ESEO Engineering School, Angers, France. From September 2007 to August 2012, he was an Associate Professor with the Mahdia Institute of Applied Science and Technology (ISSAT), Department of Electronics and Telecommunications, Tunisia. Actually, he is Associate Professor with the Electrical and Computer Engineering Department, Faculty of Engineering, King Abdulaziz University, Jeddah, Saudi Arabia.

His main research activities concern antennas, metamaterials and metasurfaces.

A Direct Solver Based on Rank-Structured Matrix for Large Arrays in Method of Moment

Weikang Yu, Hu Yang, Shengguo Li, and Yanlin Xu

College of Electronic Science and Engineering
National University of Defense Technology, Changsha, 410073, China
769280669@qq.com, yanghu90@163.com, shengguolsg@126.com, 13298656824@163.com

Abstract ─ Rank-structured matrices such as $\mathcal{H}$-matrix, $\mathcal{H}^2$-matrix and hierarchically semi-separable (HSS) have be applied to solve integral equation problems in some engineering applications. In Method of Moment (MoM), the discretization of electric field integral equation (EFIE) usually leads to a dense matrix. However, by considering the low-rank properties of off-diagonal blocks, the rank-structured theory provides a novel sparse representation for the resulting matrix. In this paper, we propose a direct solver based on one-level rank-structured matrix to analysis the electromagnetic characteristics of large arrays. The memory requirements are compared to those of direct solver and advantages of the proposed method are validated by numerical examples.

Index Terms ─ Direct solver, large arrays, rank-structured matrix.

I. INTRODUCTION

Method of Moment (MoM) is a typical numerical method to obtain the electromagnetic characteristics based on the solution of surface integral equation (SIE) [1]. Unknowns and test functions by discretization generally result in dense impedance matrix. The memory requirement of direct solver is proportional to O(N^2), with N being the matrix size. In most engineering applications, the iterative solver is commonly used owing to its high efficiency. The iterative methods based on Krylov subspace such as GMRES, BiCGStab and others depend on fast matrix-vector products. A typical application is the fast multiple method (FMM) which speeds up the matrix-vector product from O(N^2) to O($N^{1.5}$) and its improvement multilevel fast multi-pole (MLFMA) algorithm which reduces the complexity to O(Nlog$N$) [2].

Another branch of methodology is the fast direct solver which focuses on reducing the scale of the impedance matrix. Compared to iterative method, direct method does well with multiple right hand sides, which means once an efficient factorization is obtained, all right hand sides can be solved with relatively low computational cost [3]. One type of mature method based on the physical and geometrical features of targets applies fewer high order synthetic basis functions to approximate the properties of targets. The characteristic basis function method (CBF) and the synthetic basis function method (SBF) are two typical representatives [4]. Another method is based on the low-rank property of the matrix itself. Matrix compression technique like Adaptive Cross Approximation (ACA) is applied to reduce the memory requirement [5].

Hierarchical Semi-separable (HSS) matrix is a typical theory in rank-structured matrices. The term 'semi-separable' originated in the theory that if an integral kernel is approximated by an outer sum, then the system could be with a number of operations essentially determined by the order of the approximation [6]. In the same period, Greengard and Rokhlin proposed the FMM which was limited to the solution of Green's function. To some extent, HSS can be thought as the algebraic counterpart of FMM [7]. In this paper, we develop a direct solver based on one-level rank-structure matrix to analyze the electromagnetic properties of large arrays. Specifically, we maintain the information of diagonal blocks and compress the off-diagonal blocks based on the low-rank properties. The size of the compressed matrix depends on the numerical rank and influences the accuracy of solution. Finally, the remaining matrix is solved directly after ULV factorization with modest memory consumption.

II. COMPRESSION ANALYSIS

Consider the electric field integral equation (EFIE):

$$\boldsymbol{n}\times ik\eta\iint_S\left(\begin{array}{l}\boldsymbol{J}(\boldsymbol{r}')g(\boldsymbol{r},\boldsymbol{r}')\\ +\frac{1}{k^2}\nabla'\cdot\boldsymbol{J}(\boldsymbol{r}')\nabla g(\boldsymbol{r},\boldsymbol{r}')\end{array}\right)dS'=\boldsymbol{n}\times\boldsymbol{E}^{inc},\quad(1)$$

in which $g(\boldsymbol{r},\boldsymbol{r}')=\dfrac{e^{-jk|\boldsymbol{r}-\boldsymbol{r}'|}}{|\boldsymbol{r}-\boldsymbol{r}'|}$ represents Green's function, J is the induced surface current density and E^{inc} is the imposed electric field. Discretize J with a series of

Submitted On: May 9, 2017
Accepted On: September 22, 2017

RWG basis functions and get the following linear system of equations:

$$ZI = V. \tag{2}$$

The impedance matrix Z, although dense, can be thought of "data-sparse" in HSS theory. The HSS representation is a hierarchical structure and based on a recursive row or column partitioning of the matrix. The resulting matrix can be approximated in form of the multiplication of the several low dimension matrices [6, 8].

Considering a target consists of M blocks, the resulting matrix based on traditional MoM can be written as:

$$Z = \begin{pmatrix} Z_{1,1} & Z_{1,2} & \cdots & Z_{1,M} \\ Z_{2,1} & Z_{2,2} & \cdots & Z_{2,M} \\ \vdots & \vdots & \ddots & \vdots \\ Z_{M,1} & Z_{M,2} & \cdots & Z_{M,M} \end{pmatrix}. \tag{3}$$

The sub-block $Z_{i,j}$(i=1,2,…,M) represents the interaction of RWGs on block i while $Z_{i,j}$(i,j=1,2,…,M, $i \neq j$) represents the mutual relationship between block i and block j. As mentioned above, the sub-block $Z_{i,j}$ has low-rank properties and can be written approximately as:

$$Z_{i,j}^{'} = UZ_{i,j}^{c} = UU^{H}Z_{i,j}. \tag{4}$$

The U matrix is called generator which is "tall and skinny" and $Z^c_{i,j}$ is "short and wide".

In this work, we apply one-level HSS matrix theory and use the singular value decomposition (SVD) to generate the compressed form. This work is based on two facts: the numerical rank of the iterative matrix is rather small for large array and thus the storage of off-diagonal blocks can be significantly reduced. Second, the computation complexity for compression of one level HSS form is rather small compared with multiple levels of HSS. For each column, apply SVD factorization to obtain the generator U. Here, we use numerical rank r to represent the size of U and r depends on the characteristics of the normalized singular values. The whole matrix can be compressed in this form:

$$Z^{c} = \begin{pmatrix} Z_{1,1} & U_1 Z_{1,2}^{c} & \cdots & U_1 Z_{1,M}^{c} \\ U_2 Z_{2,1}^{c} & Z_{2,2} & \cdots & U_2 Z_{2,M}^{c} \\ \vdots & \vdots & \ddots & \vdots \\ U_M Z_{M,1}^{c} & U_M Z_{M,2}^{c} & \cdots & Z_{M,M} \end{pmatrix}. \tag{5}$$

In the following step, we will show how to solve the equation by applying the ULV factorization method.

III. ULV FACTRORIZATION

ULV theory arose in an effort to stabilize the fast solver for matrices characterized by a hierarchical low numerical rank structure, where U and V are orthogonal matrices and L is a lower-triangular matrix [8]. And it belongs to backward stable algorithm.

We firstly introduce the main step in ULV factorization. The generator U has the special structure:

$$U = \Pi \begin{pmatrix} I \\ E^{r} \end{pmatrix}, \tag{6}$$

where matrix Π and E^r can be obtained in advance. Construct the transformation matrix:

$$\Omega = \begin{pmatrix} -E^{r} & I \\ I & 0 \end{pmatrix} \Pi^{-1}. \tag{7}$$

We can observe that $\Omega U = \begin{bmatrix} 0 \\ I \end{bmatrix}$. Apply Ω to both off-diagonal and diagonal blocks in corresponding row blocks. Take the first row for example, we can get:

$$\Omega[Z_1\ Z_2 \ldots Z_M] = [\Omega Z_1 \begin{pmatrix} 0 \\ Z_2^{c} \end{pmatrix} \ldots \begin{pmatrix} 0 \\ Z_M^{c} \end{pmatrix}], \tag{8}$$

then partition $W = \Omega Z_1$ into $W = \begin{bmatrix} W_1 \\ W_2 \end{bmatrix}$ where W_2 has r rows. We perform an LQ factorization: $W_1 = [L\ 0]Q$. For 2×2 equation $ZI=b$, it can be transformed as:

$$\begin{aligned} \begin{pmatrix} \Omega_1 & 0 \\ 0 & \Omega_2 \end{pmatrix} Z \begin{pmatrix} Q_1^{*} & 0 \\ 0 & Q_2^{*} \end{pmatrix} &= \begin{pmatrix} [L_1\ 0] & 0 \\ W_{12}Q_1^{*} & Z^{c}{}_{1,2}Q_2^{*} \\ 0 & [L_2\ 0] \\ Z^{c}{}_{2,1}Q_1^{*} & W_{22}Q_2^{*} \end{pmatrix} \\ &= \begin{pmatrix} L_1 & 0 & 0 & 0 \\ W_{12}Q_{1;1}^{*} & W_{12}Q_{1;2}^{*} & Z_{1,2}^{c}Q_{2;1}^{*} & Z_{1,2}^{c}Q_{2;2}^{*} \\ 0 & 0 & L_2 & 0 \\ Z_{2,1}^{c}Q_{1;1}^{*} & Z_{2,1}^{c}Q_{1;2}^{*} & W_{22}Q_{2;1}^{*} & W_{22}Q_{2;2}^{*} \end{pmatrix}. \end{aligned} \tag{9}$$

For each row i, right hand sides relate to L can be solved directly:

$$Ly = \Omega b. \tag{10}$$

Then, we need to update the right-hand side by eliminated the unknowns corresponding to L:

$$b' = b - W_{i;2}Q_{i;2}^{*}y_i - \sum_{j=1,\, j\neq i}^{M} Z_c Q_{j;2}^{*}. \tag{11}$$

The remaining unknowns can be merged together to be solved in a rather small scale. The whole process is illustrated in Fig. 1.

In the end, we discuss the memory requirement in this method, which consists of two main parts: one is the main remaining unknowns and the other is the backward matrix Q for each column. Consider a linear system of N unknowns, the memory requirement of conventional MoM is $O(N^2)$. If the proposed method is applied and the system is divided into M^2 sub-blocks, the total memory requirement is $O(N^2/M+r^2M^2)$ in which r is numerical rank and generally far less than

N. Moreover, we use the compression ratio, defined as *Mr/N*, to measure the low rank properties of the off-diagonal blocks.

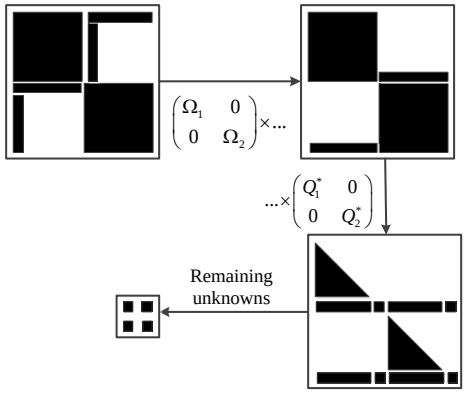

Fig. 1. Illustration of LUV factorization process.

IV. NUMERICAL RESULTS AND VALIDATION

To illustrate the validity and accuracy of the proposed method, we present several numerical examples based on EFIE. Firstly, consider a 3×3 PEC cylinder arrays as is shown in Fig. 2.

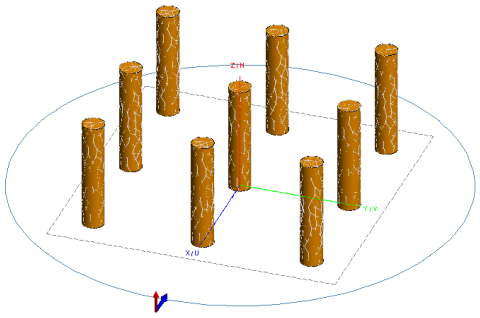

Fig. 2. Geometry of a 3×3 PEC cylinder arrays.

The excitation source is a +*z* polarized plane wave coming from x axis with frequency *f*=300 MHz. The array elements are geometrically isolated and thus the matrix will be divided into 81 sub-blocks. After discretization of the surface, 2628 triangular patches and 3942 RWG functions are defined. The size of the sub-block is 438. Before proceeding further, we first determine the numerical rank for off-diagonal blocks by setting the threshold ρ after SVD factorization. To be specific, the formulation $Err = \frac{\|I_r - I_{MoM}\|_F}{\|I_{MoM}\|_F}$ is used to illustrate the compression accuracy of the generator *U*, where "$\|\bullet\|_F$" denotes the Frobenius norm. In Table 1, we compare the current coefficient in this method with the one obtained by conventional MoM. Besides, we also show the changing tendency of current coefficients with the compression ratio.

Table 1: Relationship between compression ratio and *Err*

Threshold ρ	10^{-2}	10^{-3}	10^{-4}	10^{-5}
Compression ratio	0.05	0.14	0.22	0.32
Err	$7.2e^{-3}$	$1.4e^{-3}$	$9.1e^{-5}$	$1.7e^{-5}$

It is obvious that the numerical rank of the off-diagonal blocks can be much smaller than the original dimension, which means the memory can be reduced significantly. From the solution results, the accuracy meets the demand. Bistatic RCS of the example are calculated using the proposed method with $p=10^{-2}$, and results of Feko and MoM are also given here for comparison in Fig. 3. The memory requirement of original matrix Z is 237.1 MB. In contrast, the whole memory cost in this method is 27.4 MB.

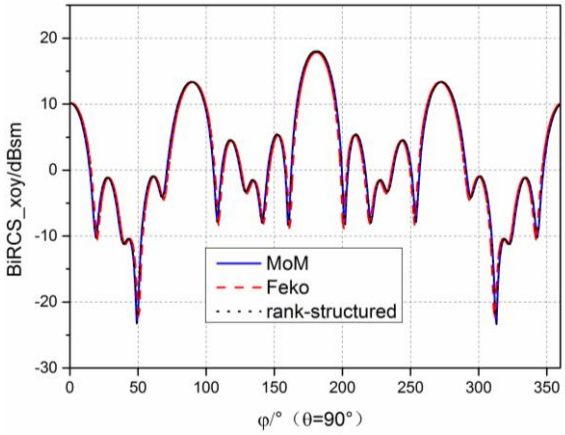

Fig. 3. Bistatic RCS of the cylinder arrays.

In fact, the rank-structured method, as purely algebraic method, is also adaptive to a single target, although the strength in memory reduction is not apparent. The second example is a PEC sphere with radius of 1 m. The excitation source is a +*z* polarized plane wave coming from x axis with frequency *f*=420 MHz A total of 7272 RWGs are defined on sphere surface. To use rank-structured method, the RWGs on the space is equally divided into 8 sub-blocks as is shown in Fig. 4. The RWGs on the connection zone are randomly distributed to sub-blocks, which has little influence on the final consequence.

Here, we just show the relationship between numerical rank and *Err* in Fig. 5. Usually, RCS results can achieve satisfying accuracy if the current coefficient error is no more than 1%.

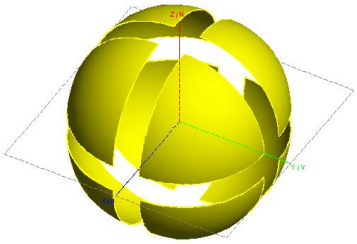

Fig. 4. Geometry of a PEC sphere after separation.

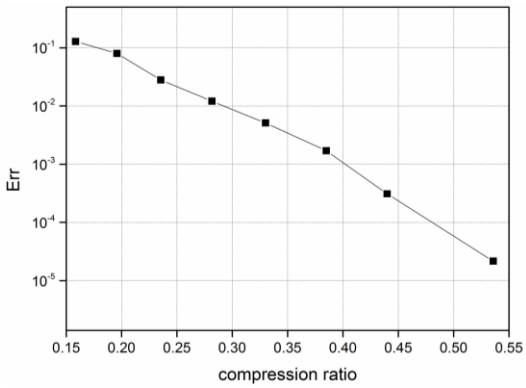

Fig. 5. Relationship between the compression ratio and *Err*.

We observe that to satisfy the accuracy of 1%, the size of reduced matrix should be about 30% of the origin matrix. In contrast, for large array in first example, the ratio of reduction can be 5% to meet the same accuracy. The reason lies in the fact that as all the groups are touching for a single target, the low-rank property is not apparent in just one-level structure. To achieve a better performance, a hierarchical and nested structure should be applied such as $\mathcal{H}^2$-matrix or HSS representation, which is our future research topic.

V. CONCLUSION

The paper proposes a memory-reduced direct method to deal with the electromagnetic problem of large scale arrays based on rank-structured theory. The method takes advantage of the low-rank properties of the impedance matrix and factorizes the matrix in form of multiplication of several low dimension matrices. The approach is perfectly suitable to the MoM and we validate this idea by two kinds of numerical results. In the end, we recommend randomized sampling algorithm [9] to generate the HSS matrix. The main advantage of this approach is that the original matrix does not need to be explicitly formed and only requires some selected elements and fast matrix-vector produce routine.

ACKNOWLEDGMENT

This work was supported by the Chinese National Science Foundation through grant No. 11401580.

REFERENCES

[1] R. F. Harrington, *Field Computation by Moment Methods*. New York: Macmillan, 1968.

[2] R. Coifman, V. Rokhlin, and S. Wandzura, "The fast multipole method for the wave equation: A pedestrian prescription," *IEEE Antennas Propag. Mag*., vol. 35, no. 3, pp. 7-12, June 1993.

[3] S. Ambikasaran and E. Darve, "An O(NlogN) fast direct solver for partial hierarchically semi-separable matrices," *[J]. Journal of Scientific Computing*, vol. 57, no. 3, pp. 477-501, 2013.

[4] L. Matekovits, G. Vecchi, G. Dassano, et al., "Synthetic function analysis of large printed structures: The solution space sampling approach," *[C]. Antennas and Propagation Society International Symposium, IEEE*, vol. 2, pp. 568-571, 2001.

[5] J. Shaeffer, "Direct solve of electrically large integral equations for problem sizes to 1 M unknowns," *[J]. IEEE Transactions on Antennas & Propagation*, vol. 56, no. 8, pp. 2306-2313, 2008.

[6] Z. Sheng, P. Dewilde, and S. Chandrasekaran, "Algorithms to solve hierarchically semi-separable systems," *[M]. System Theory, the Schur Algorithm and Multidimensional Analysis*, Birkhäuser Basel, pp. 255-294, 2007.

[7] P. Starr, "On the Numerical Solution of One-Dimensional Integral and Differential Equations," *Ph.D. thesis, Department of Computer Science*, Yale University, New Haven, CT, 1991.

[8] S. Chandrasekaran, M. Gu, and T. Pals, "A fast ULV decomposition solver for hierarchically semi-separable representations," *[J]. Siam Journal on Matrix Analysis & Applications*, vol. 28, no. 3, pp. 603-622, 2006.

[9] P. G. Martinsson, "A fast randomized algorithm for computing a hierarchically semiseparable representation of a Matrix," *[J]. SLAM Journal on Matrix Analysis & Applications*, vol. 32, no. 4, pp. 1251-1274, 2011.